Geomechanics and Engineering, *Vol. 14, No. 1 (2018) 71-81*
DOI: https://doi.org/10.12989/gae.2018.14.1.071

Stability charts and reinforcement with piles in 3D nonhomogeneous and anisotropic soil slope

Jingshu Xu*, Yongxin Li and Xiaoli Yang

School of Civil Engineering, Central South University, Changsha, 410075, China

(Received September 25, 2016, Revised June 9, 2017, Accepted June 20, 2017)

Abstract. Soils are mostly nonhomogeneous and anisotropic in nature. In this study, nonhomogeneity and anisotropy of soil are taken into consideration by assuming that the cohesion increases with depth linearly and also varies with respect to direction at a particular point. A three-dimensional rotational failure mechanism is adopted, and then a three-dimensional stability analysis of slope is carried out with the failure surface in the shape of a curvilinear cone in virtue of the limit analysis method. A quasi-static approach is used to develop stability charts in nonhomogeneous and anisotropic soils. One can easily read the safety factors from the charts without the need for iterative procedures for safety factors calculation. The charts are of practical importance to prevent a plane failure in excavation slope whether it is physically constrained or not. Then the most suitable location of piles within the reinforced slope in nonhomogeneous and anisotropic soils is explored, as well as the interactions of nonhomogeneous and anisotropic coefficients on pile reinforcement effects. The results indicate that piles are more effective when they are located between the middle and the crest of the slope, and the nonhomogeneous coefficient as well as the anisotropic coefficient will not only influence the most suitable location for piles but also affect the calculated safety factor of existing reinforced slope. In addition, the two coefficients will interact with each other on the effect on slope reinforcement.

Keywords: soil nonhomogeneity and anisotropy; three-dimensional; upper bound; piles; safety factor of slope

1. Introduction

Slope stability and slope reinforcement assessment remain an important area of study for geotechnical engineering both in theory and practice. A plenty of researches have been conducted both in slope stability analysis and existing slope reinforcement assessment (Ji and Liao 2014, Latha and Garaga 2010, Li *et al*. 2006, 2010). In aspect of natural slope stability analysis, the stability charts are drawn for slopes subjected to pore water pressure and also for those exposed to seismic forces based on the kinematic approach. The cone curve failure mechanism is proposed, with a block of width inserted into it in order to make the failure mechanism closer to the real situation. Stability charts with practical importance considered the assessment of the factor of safety of slopes without the need for an iterative procedure using a quasi-static approach (Michalowski and Dresher, 2009). Erzin and Cetin (2014) estimated the critical factor of safety value of homogeneous finite slopes employing the developed artificial neural network (ANN) and multiple regression (MR) models. Based on the nonlinear Barton-Bandis (B-B) failure criterion, Zhang (2015) conducted a plane slide rock slope stability analysis under different hydraulic distributions, and analyzed the influence of various parameters on the stability of rock slopes. Based on the lower bound theorem of limit analysis method, Zheng *et al*. (2015) derived an analytical solution for the earth retaining structures of slope subjected to complex negative influences, and presented sets of design charts for practical usage.

Slope reinforcement is another important issue for slope stability analysis (Xu 2013, Liu *et al.* 2015). In the aspect, He *et al*. (2012) conducted a seismic stability analysis of soil nail reinforced slope using the kinematic theorem of limit analysis, the critical seismic yield acceleration coefficient and the permanent displacement of slope are calculated by the objective analytical expressions, and the influence of inertial force on the stability of a nail-reinforced slope was illustrated. Based on the pseudo-static approach, Shukla and Bathurst (2012) developed an explicit analytical expression for the critical inclination of the failure plane within the soil backfill, with the consideration of tension cracks in the backfill, a uniform surcharge on the backfill, and horizontal and vertical seismic loadings. Based on a nonlinear failure criterion, Deng *et al*. (2014) conducted a limit equilibrium stability analysis of slope both in plane-strain and 3 dimensional conditions. The normal and shear stress on the slip surface are obtained and multivariate linear equations for variables determination were derived. Gao *et al*. (2015) explored the end effects of the slope failures and the effects of the pile location and diameter on the safety of the reinforced slopes in homogeneous soil.

Researches above gave references to slope stability and reinforcement effect on slope. However, these researches are aimed at homogeneous soil only. In engineering

*Corresponding author, Ph.D.
E-mail: 15207499204@163.com

ISSN: 2005-307X (Print), 2092-6219 (Online)

practical viewpoint, due to natural deposition, excavation unloading and landfill stack, cohesion force c of soil usually shows strength nonhomogeneity and anisotropy, which will influence the shear strength of soil significantly and then the stability factors of slopes. Only a few researches have been done for slope stability in nonhomogeneous and anisotropic soil slope so far. Han *et al*. (2014) investigated the three-dimensional loaded slope stability for anisotropic and nonhomogeneous slopes, and discussed the influence of factors such as the friction angel and loads on slope. Nian *et al*. (2008) analyzed the stability of a slope with reinforcing piles in anisotropic and nonhomogeneous soils using the kinematic approach of limit analysis combined with a strength reduction technique, and proposed a procedure for structural design that stabilizes the piles against landslide.

For now, no research on stability charts and reinforcement effect of three-dimensional slope in nonhomogeneous and anisotropic soil has ever been done. This paper conducts a combination research on stability charts and reinforcement effect of piles on three-dimensional slope using kinematic approach based on limit analysis method (Portioli *et al*. 2014, Clarke *et al*. 2013, Utili, 2013). In this paper, soil nonhomogeneity and anisotropy and limit analysis method are briefly reviewed, followed by the description of the three-dimensional failure mechanism used to develop the charts, which here are developed in a manner that allows for reading the safety factor without the need for iterations. Then the energy dissipation due to the resistance of piles is introduced and calculated in nonhomogeneous and anisotropic soil, then comes the parametric analysis of the most suitable location for piles within the slope and the effects of soil nonhomogeneity and anisotropy on stability of existing slope, as well as the interactions between soil nonhomogeneity and anisotropy.

2. Stability analysis of 3D nonhomogeneous soil slope

2.1 Soil nonhomogeneity and anisotropy

Soil strength is expressed by internal friction angle φ and cohesion force c in Mohr-Coulomb failure criterion. Researches show that compared with internal friction angle φ, nonhomogeneity of cohesion force c along with depth is far more obvious and strong.

In this paper, it is assumed that only the parameter c is nonhomogeneous and anisotropic, and the friction angle φ is assumed to remain homogeneous and isotropic throughout the criterion. The term 'nonhomogeneity' of cohesion implies a variation of c with respect to depth z and term 'anisotropy' of cohesion implies a variation of c with respect to direction at a particular point, as shown in Fig. 1 (b) and 1(c), respectively.

The anisotropy with respect to cohesion strength, c of the soil has been studied by several investigators and it is found that the variation of cohesion strength, c, with direction approximates to the curve shown in Fig. 1. In the following, it is assumed that the cohesion strength c_i, with its major principal stress inclined at an angle i with the vertical direction, is given by the same equation as Eq. (1)

$$c_i = c_{\mathrm{h}} + \left(c_{\mathrm{v}} - c_{\mathrm{h}}\right)\cos^2 i \tag{1}$$

where c_{h} and c_{v} are the cohesion strength in the horizontal and vertical directions respectively. The ratio of the principal cohesion strengths $c_{\mathrm{h}}/c_{\mathrm{v}}$, denoted by κ, i.e. the anisotropic coefficient, is assumed to be the same at all points in the medium. $c_i=c_{\mathrm{v}}=c_{\mathrm{h}}$ (or $\kappa=1$) is an isotropic material. Referring to Eq. (1) and Fig. 1, cohesion strength c of nonhomogeneous and anisotropic soil can be expressed as

$$c = \left(c_0 + \lambda h\right)\left(1 + \frac{1-\kappa}{\kappa}\cos^2 i\right) \tag{2}$$

where c_0 is the cohesion force in the top of slope, λ and $\kappa = c_{\mathrm{h}}/c_{\mathrm{v}}$ are the nonhomogeneous coefficient and anisotropic coefficient, respectively; $i=\theta-\pi/2-\varphi+m$, angle $m=\pi/4+\varphi/2$ is the angle between the failure plane and the plane which is normal to the direction of the major principle cohesion strength kept at an angle i with the vertical direction.

2.2 Kinematic approach

The soil is assumed to deform plastically according to the normality rule associated with the Mohr-Coulomb yield criterion by limit analysis method. The kinematic approach based on limit analysis method has been widely adopted to investigate the problems of slope stability, ultimate bearing capacity, and other geotechnical problems (Pan and Dias 2016, 2017, Yang 2017, Yang and Zhang 2017). The kinematic approach of limit analysis states that the rate of internal work is not less than the work rate of body force, namely

$$\int_V \sigma^*_{ij}\dot{\varepsilon}^*_{ij}\,dV \geq \int_S T_i v_i\,dS + \int_V X_i v_i^*\,dV \tag{3}$$

where $\dot{\varepsilon}_{ij}$ is strain rate, v_i is the velocity along the velocity discontinuity surface, v_i^* is the velocity vector in the kinematically admissible mechanism, $v_i^*=v_i^*$ on boundary S (given boundary condition), σ^*_{ij} is stress, S and V are the slope boundary and volume respectively. The details of this method to stability problems can be found in Ref. in Refs (Michalowski *et al.* 2009, 2011, Yang *et al*. 2017, Yang 2017, Yang and Yao 2017).

2.3 Failure mechanism of 3D nonhomogeneous soil slope

In this three-dimensional failure mechanism, cohesion force c increases along with the slope height H, as shown in Fig. 1 and Eq. (2).

The three-dimensional rotational failure mechanism has the shape of a curvilinear cone with vertex angle 2φ. In this rotational failure mechanism, the stability factor is determined by three variables r'_0/r_0, θ_0 and θ_{h}. It is only one part of this surface that intersects the slope and the trace of

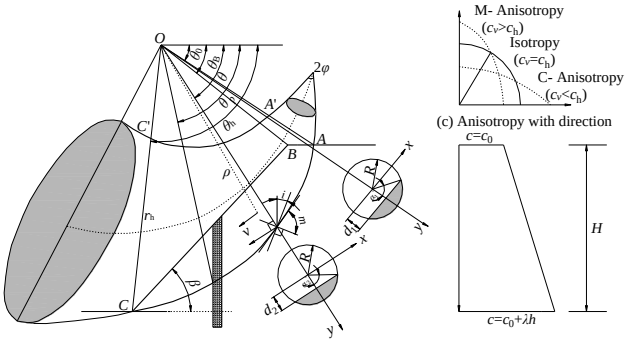

(a) 3 dimensional rotating failure mechanism (b) Nonhomogeneity with depth

Fig. 1 Three-dimensional failure mechanism for a nonhomogeneous and anisotropic slope

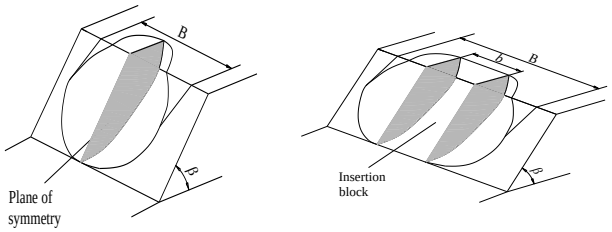

(a) 3D failure mechanism without plane insert (b) 3D failure mechanism with plane insert

Fig. 2 Three-dimensional rotational failure mechanism: (a) without plane insert; (b) with plane insert

this surface go through the toe point D. The discontinuity surface of the mechanism on the symmetry plane is described by two log-spirals, *AD*

$$r = r_0 e^{(\theta-\theta_0)\tan\varphi} \tag{4}$$

and *A′D′*

$$r' = r_0' e^{-(\theta-\theta_0)\tan\varphi} \tag{5}$$

As shown in Fig. 1, $OA=r_0$, $O'A'=r'_0$. The distance from rotation center O to the cone axis is r_m, and the cross section of a cone is a circle with radius *R*. The equations are as follows

$$r_m = (r+r')/2 = r_0 f_1 \tag{6}$$

$$R = (r-r')/2 = r_0 f_2 \tag{7}$$

where f_1 and f_2 are given in the Appendix.

Previous research showed that stability factor is related with not only the slope angle and strength parameters *c* and φ, but also the width of sliding block (Michalowski and Dresher 2009). In order to make the result consistent with practice, a block of width *b* is inserted into the mechanism, as shown in Fig. 2. When the width of the insert block $b\to\infty$, solution of plane-strain failure mechanism is equal to the solution of three-dimensional failure mechanism. The insert block also adds the optimization of the stability factor a new variable *b* by introducing the width *B* as restrictive conditions, and the sum of the width of three-dimensional mechanism and insertion block cannot be larger than the limit width *B*.

2.4 Work and energy calculations

2.4.1 Internal energy dissipation

Section θ_0-θ_B of rotating body

The cohesion force *c* of any point on the arc in section θ_0-θ_B is

$$c_{0-B} = (c_0+\lambda h)\left(1+\frac{1-\kappa}{\kappa}\cos^2 i\right) = \left[c_0+\lambda R(\cos\alpha-\cos\alpha_1^*)\sin\theta\right]\left(1+\frac{1-\kappa}{\kappa}\cos^2 i\right) \tag{8}$$

Then, interior energy dissipation of section θ_0–θ_B is

$$\begin{aligned} D_{\text{AB-3D}} &= 2\omega\int_{\theta_0}^{\theta_B}\int_0^{\alpha_1^*} c_{0-B}R(r_m+R\cos\alpha)^2 d\alpha d\theta \\ &= \omega c_0 r_0^3 g_1 + \omega\lambda r_0^4 g_2 \end{aligned} \tag{9}$$

where $\alpha_1^*=\arccos(d_1/R)$, $d_1=\frac{r_0\sin\theta_0}{\sin\theta}-r_m=r_0 f_3$ and f_3 is given in the Appendix.

Section θ_B-θ_h of rotating body

The cohesion force *c* on the arc of the section θ_B-θ_h is

$$c_{B-C} = \left[c_0+\lambda(r\sin\theta-r_0\sin\theta_0)+\lambda R(\cos\alpha-\cos\alpha_2^*)\sin\theta\right]\left(1+\frac{1-\kappa}{\kappa}\cos^2 i\right) \tag{10}$$

Then, interior energy dissipation of section θ_B-θ_h is

$$\begin{aligned} D_{\text{BC-3D}} &= 2\omega\int_{\theta_B}^{\theta_C}\int_0^{\alpha_2^*} c_{B-h}R(r_m+R\cos\alpha)^2 d\alpha d\theta \\ &= \omega c_0 r_0^3 g_3 + \omega\lambda r_0^4 (g_4+g_5) \end{aligned} \tag{11}$$

where $\alpha_2^*=\arccos(d_2/R)$, $d_2=r_0 f_4$ and f_4 is given in the Appendix.

The sum of the internal energy dissipation of rotating body can be expressed as follows

$$D_{3D} = \omega c_0 r_0^3 (g_1+g_3) + \omega\lambda r_0^4 (g_2+g_4+g_5) \tag{12}$$

where g_1 to g_5 are given in the Appendix.

Insertion block

The internal energy dissipation of insertion block with width *b* can be expressed as follows

$$\begin{aligned} D_{\text{insert-3D}} &= b\int_{S_1} c\cos\varphi[v]dS_1 = b\omega r_0^2\int_{\theta_0}^{\theta_h}\left[c_0+\lambda(r\sin\theta-r_0\sin\theta_0)\right]\exp\left[2(\theta-\theta_0)\tan\varphi\right]d\theta \\ &= \omega c_0 r_0^3 g_6 + \omega\lambda r_0^4 g_7 \end{aligned} \tag{13}$$

The total internal energy dissipation rate *D* can be expressed as

$$D = D_{3D} + D_{\text{insert-3D}} = \omega c_0 r_0^3 (g_1+g_3+g_6) + \omega\lambda r_0^4 (g_2+g_4+g_5+g_7) \tag{14}$$

where g_6 and g_7 are given in the Appendix.

2.4.2 External work rates

On the arbitrary cross section of the failure mechanism, the local coordinate system *xOy* is established (axis *x* is perpendicular to the paper), as shown in Fig. 1. The velocity *v* can be expressed as

$$v = (r_m+y)\omega \tag{15}$$

where ω is the angular velocity, and the infinitesimal work rate element is

$$dw = \gamma v\cos\theta dV = \gamma v\cos\theta dxdy(r_m+y)d\theta \tag{16}$$

For three-dimensional rotational mechanism, the work rate of the soil weight can be written as

$$W_{\gamma-3D}=2\omega\gamma[\int_{\theta_0}^{\theta_B}\int_0^{x_1^*}\int_{d_1}^{y^*}(r_m+y)^2\cos\theta dxdyd\theta+\int_{\theta_B}^{\theta_h}\int_0^{x_2^*}\int_{d_2}^{y^*}(r_m+y)^2\cos\theta dxdyd\theta] \quad (17)$$

According to the geometric relations in Fig. 1, the integration limits along y is $y^*=\sqrt{R^2-x^2}$ and the integration limits along x is $x_i^*=\sqrt{R^2-d_i^2}$ (i=1, 2), d_i can be written as

$$d_1=\frac{\sin(\theta_0+\alpha)}{\sin(\theta+\alpha)}r_0-r_m=r_0f_3(\theta) \quad (18)$$

$$d_2=\frac{\sin(\theta_h+\beta)}{\sin(\theta+\beta)}r_0e^{(\theta_h-\theta_0)\tan\varphi}-r_m=r_0f_4(\theta) \quad (19)$$

Based on trigonometric relations, angle θ_B can be expressed as

$$\theta_B=\arctan\frac{\sin\theta_0}{\cos\theta_0-\zeta} \quad (20)$$

$$\zeta=\frac{\sin(\theta_h-\theta_0)}{\sin\theta_h}-\frac{e^{(\theta_h-\theta_0)\tan\varphi}\sin\theta_h-\sin\theta_0}{\sin\theta_h\sin\beta}\sin(\theta_h+\beta) \quad (21)$$

Eq. (17) can be briefly written as

$$W_{\gamma-3D}=\gamma\omega r_0^4g_8 \quad (22)$$

For insertion block, the work rate of the soil weight can be written as

$$W_{\gamma-insert}=\gamma\omega r_0^4g_9 \quad (23)$$

where g_8 and g_9 are given in the Appendix.

By equating internal energy dissipation to external work rate, the critical height of nonhomogeneous soil slope can be obtained

$$H=\frac{c_0}{\gamma}\left[e^{(\theta_h-\theta_0)\tan\varphi}\sin\theta_h-\sin\theta_0\right]\frac{g_1+g_3+g_6}{g_8+g_9-\frac{\lambda}{\gamma}(g_2+g_4+g_5+g_7)} \quad (24)$$

The minimum upper solution of critical height of slope in nonhomogeneous and anisotropic soil can be obtained by optimization to Eq. (24).

Table 1 Comparison of present solution with Michalowski and Drescher (2009)

B/H	The results	$\beta_1=\beta_2$/°				
		30	45	60	75	90
1.5	Michalowski	32.35	16.64	11.75	8.56	7.12
	Present solution	32.42	16.46	11.85	9.30	7.66
2.0	Michalowski	28.91	14.88	10.53	8.17	6.80
	Present solution	28.97	15.27	10.98	8.59	6.90
3.0	Michalowski	25.69	13.73	9.75	7.50	6.01
	Present solution	26.22	14.13	10.14	7.87	6.21
5.0	Michalowski	23.84	12.98	9.27	7.08	5.50
	Present solution	24.37	13.23	9.49	7.32	5.70
10.0	Michalowski	22.69	12.49	8.93	6.81	5.23
	Present solution	23.04	12.62	9.07	6.94	5.35

2.4.3 Optimization for stability factor

Based on Mohr-Coulomb failure criterion, critical height of a slope in nonhomogeneous and anisotropic soil is related to the parameters of θ_0, θ_h, r'_0/r_0 and B/H. In order to make failure mechanism geometrically meaningful, the above parameters must satisfy the following constraint conditions.

$$\begin{cases}0<\theta_0<\theta_B<\theta_h<\pi\\0<r_0^{'}/r_0<1\\0<\left(b+B_{max}^{'}\right)/H<B/H\end{cases} \quad (25)$$

Stability factor N_s of slope in nonhomogeneous and anisotropic soil is defined as

$$N_s=\gamma H_c/c_0 \quad (26)$$

where H_c is the critical height by optimization as follows:

With respect to the constraint conditions and non-negativity of the external work rate by soil weight and the internal energy dissipation, stability factors of three-dimensional slopes are calculated on the basis of all the possible sets of the independent variables θ_0, θ_h and r'_0/r_0. Then the best fit stability factor (the minimum one, for that it is an upper bound solution) will be found finally through the search of all the solutions obtained under all the possible sets of the independent variables.

2.4.4 Comparisons

When the anisotropy coefficient κ=1 and the nonhomogeneous coefficient λ=0, the three-dimensional nonhomogeneous and anisotropic slope reduces to a homogeneous and isotropic one. For comparison with the results by Michalowski and Drescher (2009), the stability factor $\gamma H_c/c_0$ of slope without reinforcement is calculated and listed in Table 1. Agreement shows that the solutions presented in this paper are effective.

3. Stability charts for nonhomogeneous and anisotropic soil slope

One can estimate the stability condition of slope directly from the safety factor. So, from a practical stand point, it is the slope safety factor that is of more interest to engineers than dimensionless critical height $\gamma H_c/c_0$. The safety factor is defined as

$$F_s=\frac{c}{c_m}=\frac{\tan\varphi}{\tan\varphi_m} \quad (27)$$

where the strength parameters c_m and φ_m are the minimum parameters required to maintain limit equilibrium.

In order to obtain the minimum F_s, a dichotomy procedure similar to the optimization process for the stability factors is carried out with respect to the unknown parameters (θ_0, θ_h, r'_0/r_0, and b/B) describing the slip surface as

$$F_s=\min f\left(F_s,\theta_0,\theta_h,r_0'/r_0,b/B\middle|c,\varphi,\gamma,H,B,\beta,\lambda,\kappa\right) \quad (28)$$

where H is the slope height, β is the slope angle, B is the

slope width and λ and κ are the nonhomogeneous and anisotropy coefficients, respectively.

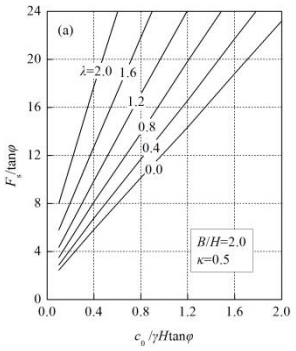

(a)

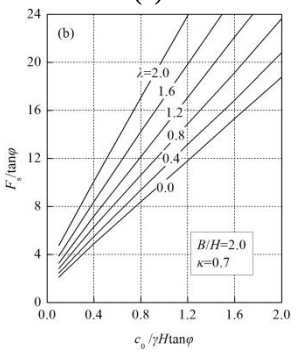

(b)

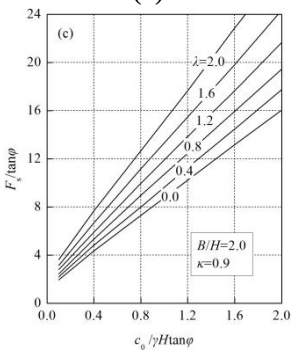

(c)

Fig. 3 Stability charts for nonhomogeneous and anisotropic soil slope for B/H=2.0: (a) κ=0.5, (b) κ=0.7 and (c) κ=0.9. $c_0/\gamma H\tan\varphi$, dimensionless parameter

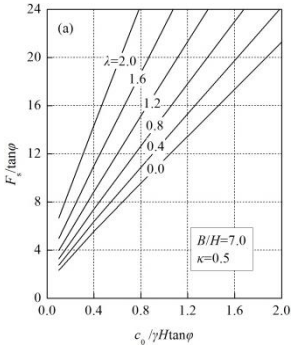

(a)

Fig. 4 Stability charts for nonhomogeneous and anisotropic soil slope for B/H=7.0: (a) κ=0.5, (b) κ=0.7 and (c) κ=0.9. $c_0/\gamma H\tan\varphi$, dimensionless parameter

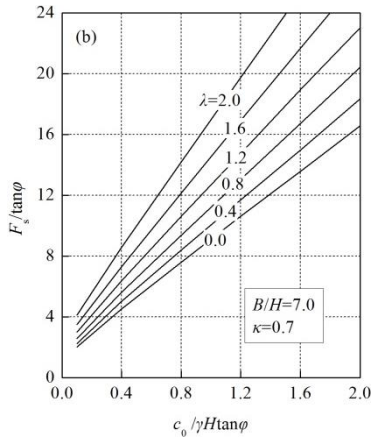

(b)

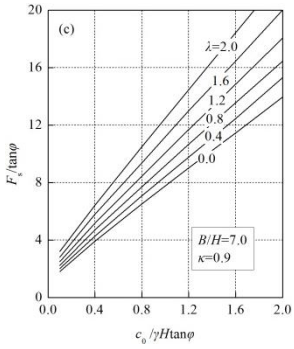

(c)

Fig. 4 Continued

To avoid iteration, the results of safety factor need to be presented as the function of a parameter independent of the safety factor and $c_0/\gamma H\tan\varphi$ is chosen here to make this parameter dimensionless. This had been done previously for both plane strain and three-dimensional analyses (Ito and Matsui 2011). A slope with a 60° inclination angle and two different ratios B/H=2.0 and 7.0 is considered here and the results are presented in the charts in Figs. 3 and 4. Each curve in one chart represents the coefficient $Fs/\tan\varphi$ with a specific nonhomogeneous coefficient λ ranging from 0 to 2.0.

As expected, safety factor of the slope increases with increasing nonhomogeneous coefficient λ and decreases with increasing anisotropic coefficient κ and ratio B/H. Besides, curves in one every specific chart get more intensive as κ increasing, which indicates that coefficient κ has an impact on soil nonhomogeneity. Thus, the enhancement of soil anisotropy will weaken the effect of soil nonhomogeneity on slope stability. However, change of ratio B/H makes no difference on effect of soil nonhomogeneity on slope stability.

The charts in Figs. 3 and 4 are convenient to use with a determined coefficient $c_0/\gamma H\tan\varphi$ for an existing slope and the value of $F_s/\tan\varphi$ is read from an appropriate chart. For example, for a slope of height H=15m and limited in width to 30 m (B/H=2.0) and β=60°, γ=22 kN/m^3, c_0=30 kN/m^2, φ=10°, nonhomogeneous coefficient λ=1.6 and anisotropic coefficient κ=0.7, calculated coefficient $c_0/\gamma H\tan\varphi$=0.516, and from the chart in Fig. 3, $F_s/\tan\varphi$=10.12, leading to $F_s\approx$1.784.

4. Slope reinforced with piles in nonhomogeneous and anisotropic soil

A new energy balance equation of work rate is written based on the three-dimensional failure mechanism when the slope is reinforced with a row of piles and then an upper-bound solution can be derived from the balance equation. An additional rate of energy dissipation done by the resistance of the piles D_p must be counted in the balance equation of work rate as

$$W_\gamma = D_{int} + D_p \tag{28}$$

where W_γ is the external work rate by soil weight, D_{int} and D_p are the internal energy dissipations by soil and the resistance of the piles respectively, D_p is calculated below.

4.1 Dissipation due to resistance of piles

For frictional and cohesive soils ($\varphi\neq0$, $c\neq0$), the equations for estimating the lateral forces acting on a row of piles presented by Ito and Matsui (2011) is written as follows

$$\begin{aligned} p(z) = c_h A\Bigg(&\frac{1}{N_\varphi\tan\varphi}\left\{\exp\left[\frac{D_1-D_2}{D_2}N_\varphi\tan\varphi\tan\left(\frac{\pi}{8}+\frac{\varphi}{4}\right)\right]-2N_\varphi^{1/2}\tan\varphi-1\right\} \\ &+\frac{2\tan\varphi+2N_\varphi^{1/2}+N_\varphi^{-1/2}}{N_\varphi^{1/2}\tan\varphi+N_\varphi-1}\Bigg)-c_h\left(D_1\frac{2\tan\varphi+2N_\varphi^{1/2}+N_\varphi^{-1/2}}{N_\varphi^{1/2}\tan\varphi+N_\varphi-1}-2D_2N_\varphi^{-1/2}\right) \\ &+\frac{\gamma z}{N_\varphi}\left\{A\exp\left[\frac{D_1-D_2}{D_2}N_\varphi\tan\varphi\tan\left(\frac{\pi}{8}+\frac{\varphi}{4}\right)\right]-D_2\right\} \end{aligned} \tag{29}$$

where c_h is the horizontal cohesion of soil; D_1 and D_2 are the center-to-center spacing and the opening between piles; (D_1-D_2) is the pile diameter; γ is the unit weight of soil; z is the depth of soil layer from the ground surface; $N_\varphi=\tan(\pi/4+\varphi/2)$. The strength parameters c and φ are also reduced by F_s in the equation of the lateral force of piles $p(z)$.

The rate of energy dissipation due to the resistance of the piles, D_p, equals the pile lateral force $p(z)$ in the active area (Fig. 5) multiplied by the instantaneous velocity at the point of $p(z)$. And the instantaneous velocity at the point of $p(z)$ equals the product of the angular velocity ω and the arm of lateral force $p(z)$ to point O.

4.2 Comparison with 2D condition

In order to verify the effectiveness of the method performed in this paper, the nonhomogeneous and anisotropic soil slope turn into a homogeneous one by assigning the nonhomogeneous coefficient $\lambda=0$ and anisotropy coefficient $\kappa=1$. Then two different conditions of three-dimensional slope reinforcement are calculated and compared with the two dimensional results by Li *et al.* (2006) in Fig. 6. It is obvious that when the ratio $B/H\geq5.0$, the differences between the three-dimensional results by this paper and the two dimensional condition are less than 20%, which means the results obtained in this paper are effective and acceptable. In Fig. 6, the location of piles is assumed varies between the toe and the top of the slope, and the safety factors are calculated and plotted against the dimensionless abscissa X_F/L_x, where $L_x=H/\tan\beta$, as shown in Fig. 5.

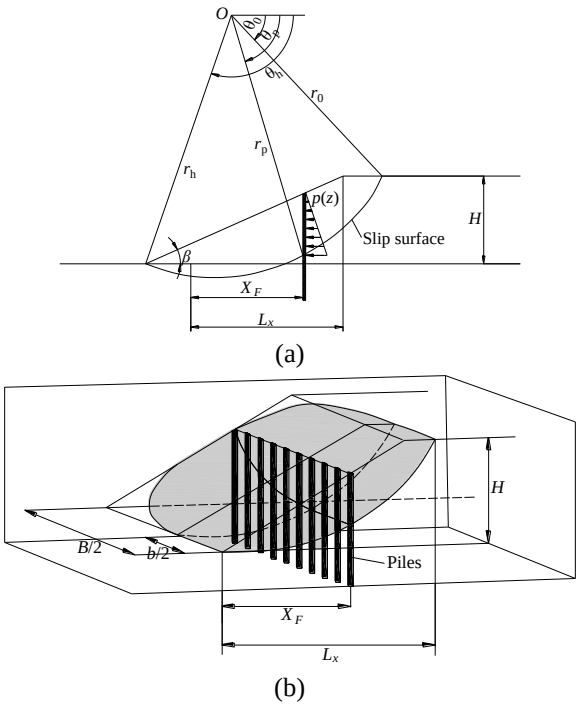

Fig. 5 Piles location for three-dimensional nonhomogeneous and anisotropic slope

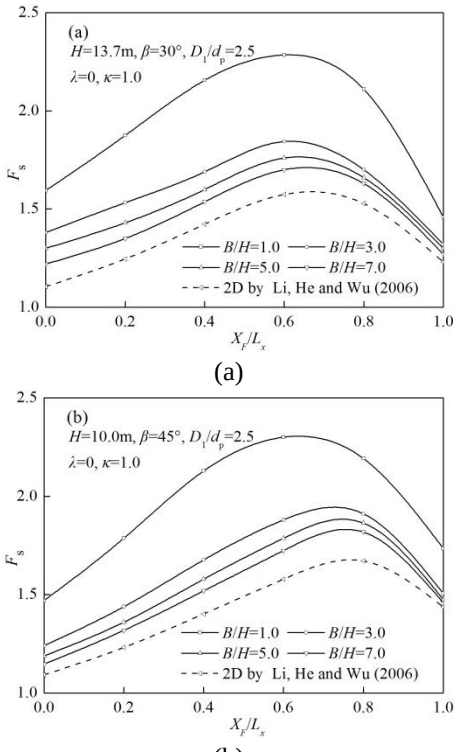

Fig. 6 Comparison with two dimensional solution

5. Numerical results and discussions

5.1 Suitable location of piles within slope

The influence of the location of piles, X_F, on the safety factor of the slope is an important issue, and in order to

illustrate the influence of the pile location, X_F, on slope stability, a slope with β=60° is considered. The most suitable position for the piles is where the piles are most effective for improving slope stability, namely, the value of F_s.

As can be seen from Fig. 7, the safety factor, F_s, changes evidently with varying positions of the piles within the slope. The piles are more effective when they are located between the middle and the crest of the slope. Besides, from Fig. 7, it is found that the increase of nonhomogeneous coefficient λ and the decrease of the anisotropic coefficient κ will not only improve the stability of slope but also make the most suitable location of piles move upward to the slope crest; the change of only one coefficient, no matter λ or κ, can only influence the slope stability status, but has no impact on the most suitable location of the piles. From Fig. 7, it is also found that decrease of κ will enhance the effect of soil nonhomogeneity, especially nearby the area of the most suitable location.

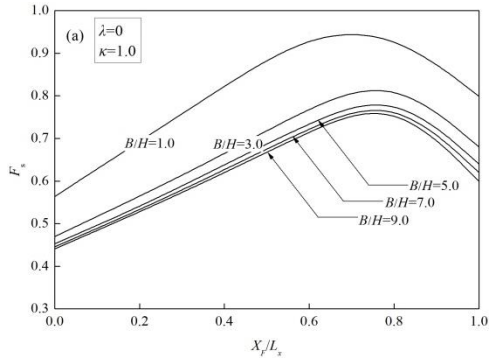

(a)

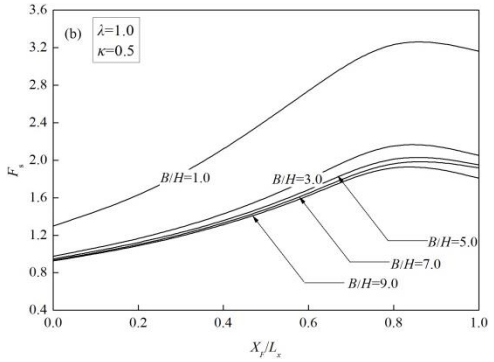

(b)

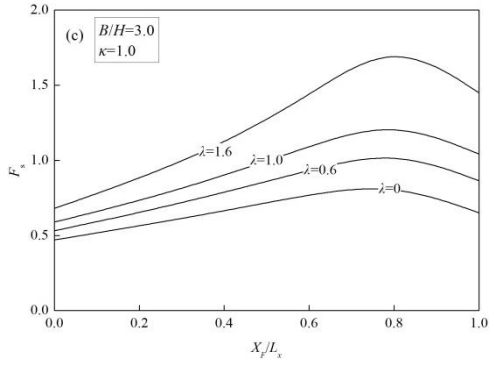

(c)

Fig. 7 The most suitable location of piles within slope

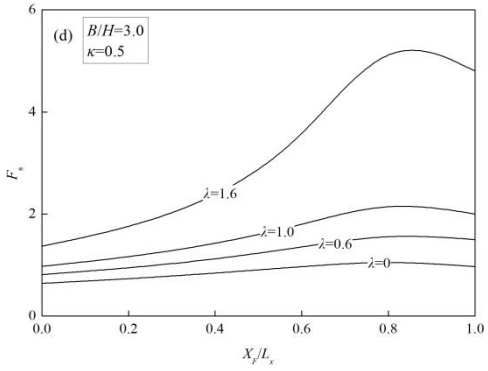

(d)

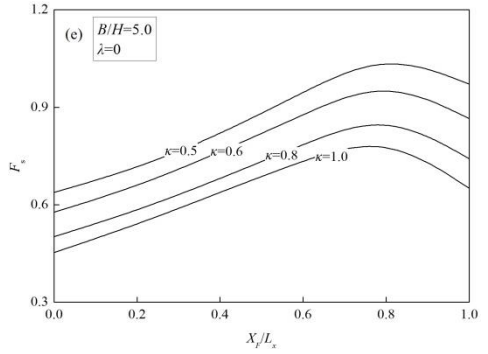

(e)

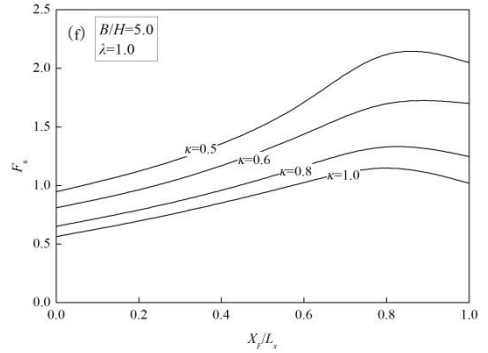

(f)

Fig. 7 Continued

5.2 Effect of soil nonhomogeneity on slope stability

To demonstrate the effect of soil nonhomogeneity on slope stability, Fig. 8 presents the values of safety factor in different pile locations X_F/L_x=0, 0.4 and 0.8 respectively in nonhomogeneous and anisotropic soil slope with slope angle β=60°, h=13.7 m, γ=19.63 kN/m^3, c_0=10 kPa, φ=10° and the nonhomogeneous coefficient λ ranging from 0 to 2.0. Curves in the first three Fig. 8(a)-8(c) and the last three ones Fig. 8(d)-8(f) represent the slope stability status under different ratios B/H and coefficient κ respectively.

Among the first three Fig. 8(a)-8(c), the effect of soil nonhomogeneity on enhancing the slope stability is the most significant round the most suitable piles location (X_F/L_x=0.8) and within a narrow slope width (B/H=1), while the plane-strain condition (B/H=9) has the least significant effect. Besides, in the last three Fig. 8(d)-8(f), the effect of soil nonhomogeneity on slope stability becomes more significant as the coefficient κ decreasing

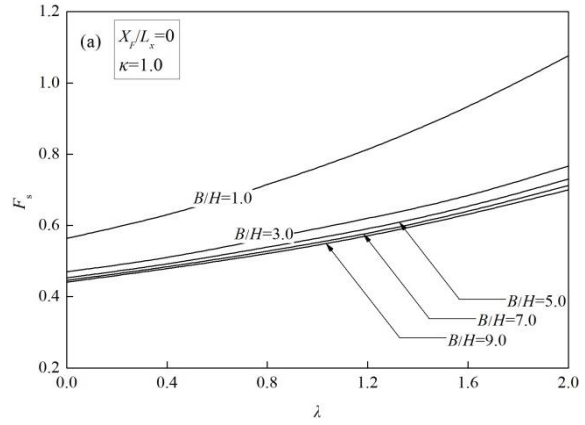

(a)

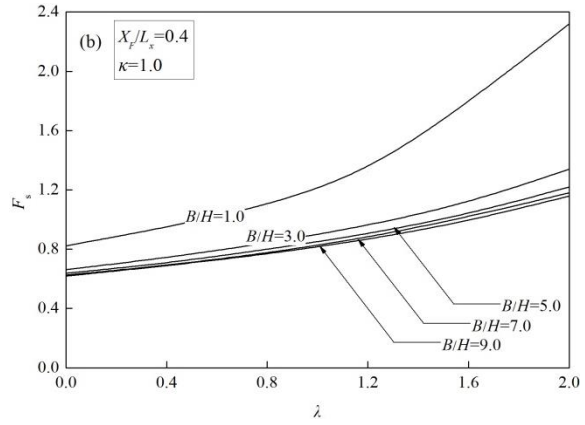

(b)

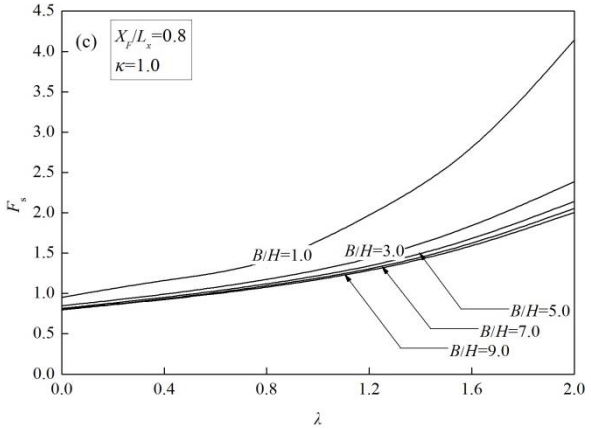

(c)

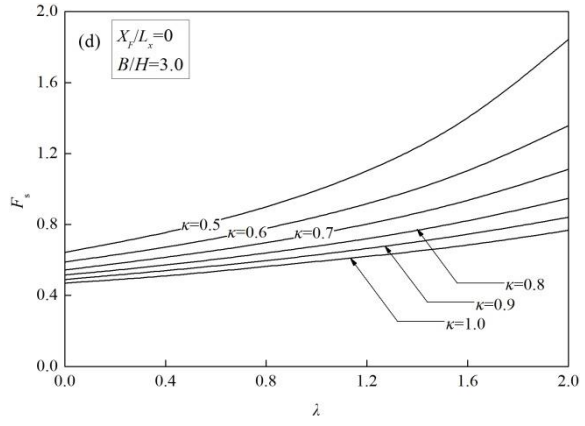

(d)

Fig. 8 Effect of soil nonhomogeneity on slope stability

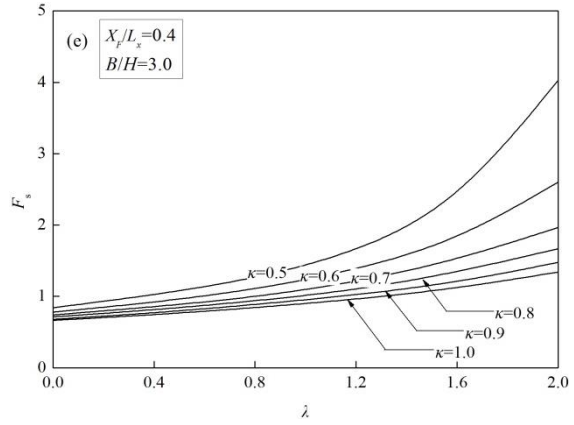

(e)

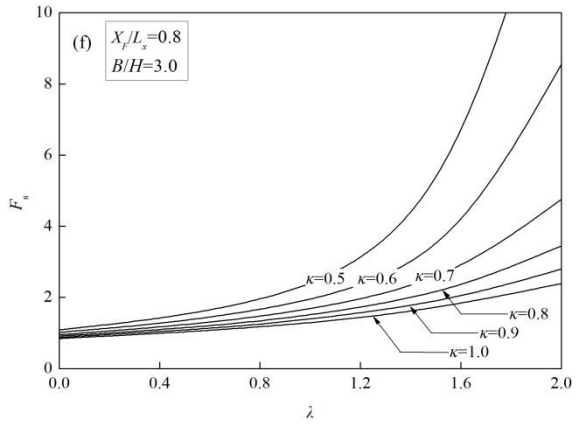

(f)

Fig. 8 Effect of soil nonhomogeneity on slope stability

and X_F/L_x approaching the most suitable piles location. In Fig. 8(f), the safety factor F_s increases from 1.019 to 1.25 when coefficient λ changes from 0 to 0.4, and then F_s increases from 3.62 to 8.55 when coefficient λ changes from 1.6 to 2.0 under the same anisotropic coefficient κ=0.6, which means the effect of soil nonhomogeneity on slope stability are becoming more and more stronger with the increase of the coefficient λ itself.

5.3 Effect of soil anisotropy on slope stability

To demonstrate the effect of soil anisotropy on slope stability, Fig. 9 presents the values of safety factor in different pile locations X_F/L_x=0, 0.4 and 0.8 respectively for the example slope with the anisotropic coefficient κ ranging from 0.5 to 1.0. Curves in the first three Fig. 9(a)-9(c) and the last three ones Fig. 9(d)-9(f) represents the slope stability status under different ratios B/H and coefficient λ respectively.

Curves among the first three Fig. 9(a)-9(c) are approximately parallel to each other, indicating that the difference in decrease of the safety factor is independent of the value of B/H. It is also clear that when the slope is constrained to a narrow width B/H=1.0, the reinforcement effects of the piles are more significant.

Besides, in Fig. 9(d)-9(f), the effect of soil anisotropy on slope stability becomes more significant as the coefficient λ increasing and X_F/L_x approaching the most suitable piles

location, namely the stronger the soil nonhomogeneity is, the more effective the soil anisotropy on slope stability will be.

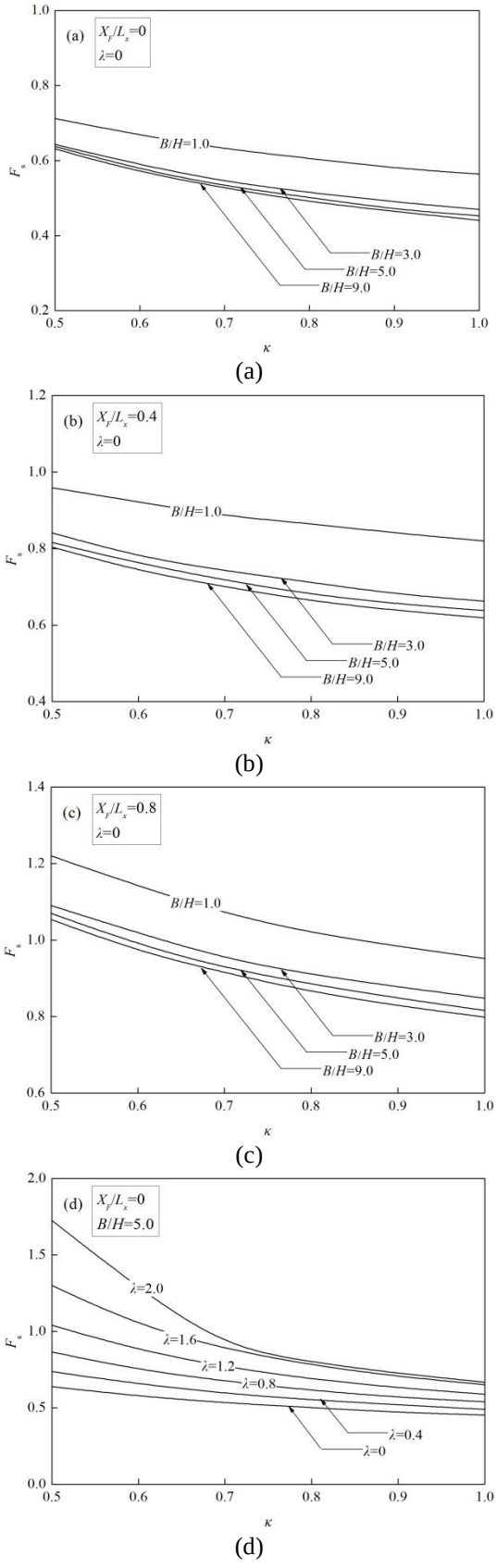

Fig. 9 Effect of soil anisotropy on slope stability

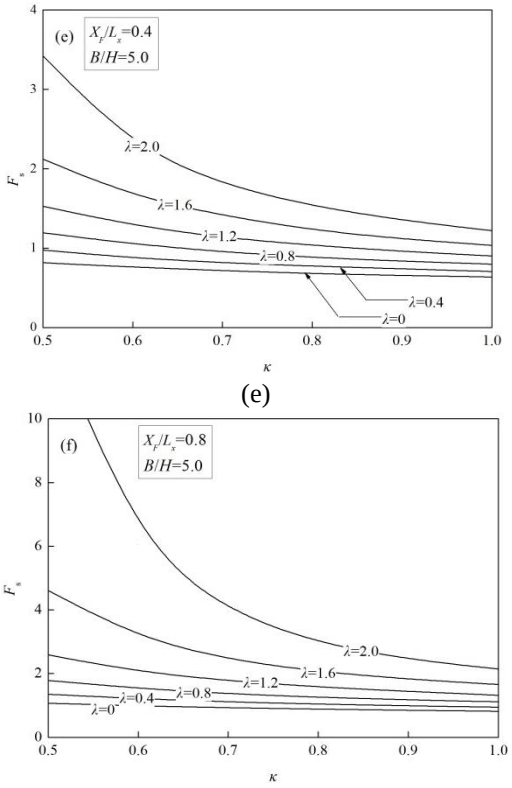

Fig. 9 Continued

6. Conclusions

Soils in nature are mostly nonhomogeneous and anisotropic. Soil is assumed to be nonhomogeneous and anisotropic in this paper that the cohesion increases with depth and also varies with respect to direction at a particular point. Based on the kinematic approach of limit analysis, a set of charts were presented for the assessment of the stability of unreinforced slopes. These charts can be conveniently used for slope stability assessment in nonhomogeneous and anisotropic soil. Then the most suitable location of piles within the reinforced slope in nonhomogeneous and anisotropic soil is explored, as well as the interactions of soil nonhomogeneity and anisotropy on pile reinforcement effects. The main conclusions are drawn as follows

• Stability charts in this paper are convenient to use for natural slope stability assessment in nonhomogeneous and anisotropic soil, the usage of the charts is also given by an example.

• The most suitable reinforcement location for piles is located between the middle and the crest of the slope, and the increase of nonhomogeneous coefficient λ and decrease of the anisotropic coefficient κ will not only improve the stability of slope but also make the most suitable location of piles moves upward to the slope crest; change of only one coefficient, no matter λ or κ, can only influence the slope stability status, but has no impact on the most suitable location of piles.

• The reinforcement effect of piles in a given location is affected by the two coefficients λ and κ significantly,

especially the nonhomogeneous coefficient λ. The growth rate of the impact of soil nonhomogeneity on slope stability will be stronger as λ getting larger.

• There is an interaction between the nonhomogeneous coefficient λ and the anisotropic coefficient κ. Decrease of κ will enhance the effect of soil nonhomogeneity, especially within the area of the most suitable location, besides, it is also found that the stronger the soil nonhomogeneity is, the more effective the soil anisotropy on slope stability will be.

Acknowledgments

The preparation of the paper has received financial supports from National Basic Research 973 Program of China (2013CB036004), Innovation Foundation for Postgraduate of Central South University, China (2015zzts061), National Natural Science Foundation of China (51378510) and the National Natural Science Foundation of China (51408180). The financial supports are greatly appreciated.

References

Clarke, S.D., Smith, C.C. and Gilbert, M. (2013), "Modelling discrete soil reinforcement in numerical limit analysis", *Can. Geotech. J.*, **50**(7), 705-715.

Deng, D.P., Zhao, L.H. and Li, L. (2014), "Limit equilibrium slope stability analysis using the nonlinear strength failure criterion", *Can. Geotech. J.*, **52**(5), 563-576.

Erzin, Y. and Cetin, T. (2014), "The Prediction of the critical factor of safety of homogeneous finite slopes subjected to earthquake forces using neural networks and multiple regressions", *Geomech. Eng.*, **6**(1), 1-15.

Gao, Y.F., Ye, M. and Zhang, F. (2015), "Three-dimensional analysis of slopes reinforced with piles", *J. Centr. South U.*, **22**(6), 2322-2327.

Han, C.Y., Chen, J.J. and Xia, X.H. (2014), "Three-dimensional stability analysis of anisotropic and non-homogeneous slopes using limit analysis", *J. Centr. South U.*, **21**(3), 1142-1147.

He, S., Ouyang, C.J. and Luo, Y. (2012), "Seismic stability analysis of soil nail reinforced slope using kinematic approach of limit analysis", *Environ. Earth Sci.*, **66**(1), 319-326.

Ito, T. and Matsui, T. (2011), "Design method for stabilizing piles against landslide-one row of piles", *Soil Found.*, **21**(1), 21-37.

Ji, J. and Liao, H.J. (2014), "Sensitivity-based reliability analysis of earth slopes using finite element method", *Geomech. Eng.*, **6**(6), 545-560.

Latha, G.M. and Garaga, A. (2010) "Stability analysis of a rock slope in Himalayas", *Geomech. Eng.*, **2**(2), 125-140.

Li, X.P., He, S.M. and Wang, C.H. (2006), "Stability analysis of slopes reinforced with piles using limit analysis method", *Adv. Earth. Struct.*, **9**(151), 105-112.

Li, X.P., He, S.M. and Wu, Y. (2010), "Seismic displacement of slopes reinforced with piles", *J. Geotech. Geoenviron. Eng.*, **136**(6), 880-884.

Liu, Y.R., Wu, Z.S., Chang, Q., Li, B. and Yang, Q. (2015), "Stability and reinforcement analysis of rock slope based on elasto-plastic finite element method", *J. Centr. South U.*, **22**(7), 2739-2751.

Michalowski, R.L. and Dresher, A. (2009), "Three-dimensional stability of slopes and excavations", *Géotechnique*, **59**(10), 839-850.

Michalowski, R.L. and Martel, T. (2011), "Stability charts for 3d failures of steep slopes subjected to seismic excitation", *J. Geotech. Geoenviron. Eng.*, **137**(2), 183-189.

Nian, T.K., Chen, G.Q. and Luan, M.T. (2008), "Limit analysis of the stability of slopes reinforced with piles against landslide in nonhomogeneous and anisotropic soils", *Can. Geotech. J.*, **45**(8), 1092-1103.

Pan, Q.J. and Dias, D. (2016), "The effect of pore water pressure on tunnel face stability", *J. Numer. Anal. Met. Geomech.*, **40**(15), 2123-2136.

Pan, Q.J. and Dias, D. (2017), "Upper-bound analysis on the face stability of a non-circular tunnel", *Tunn. Undergr. Sp. Technol.*, **62**, 96-102.

Portioli, F., Casapulla, C., Gilbert, M. and Cascini, L. (2014), "Limit analysis of 3D masonry block structures with non-associative frictional joints using cone programming", *Comput. Struct.*, **143**, 108-121.

Shukla, S.K. and Bathurst, R.J. (2012), "An analytical expression for the dynamic active thrust from *c-φ* soil backfill on retaining walls with wall friction and adhesion", *Geomech. Eng.*, **4**(3), 209-218.

Utili, S. (2013), "Investigation by limit analysis on the stability of slopes with cracks", *Géotechnique*, **63**(2), 140-154.

Xu, J.C. (2013), "Analytic hierarchy process for assessing factors influencing the stability of soil slopes reinforced with piles", *Environ. Earth Sci.*, **70**(4), 1507-1514.

Yang, X.L. (2017), "Effect of pore-water pressure on 3D stability of rock slope", *Int. J. Geomech.*, 17(9), 06017015.

Yang, X.L. (2018), "Lower bound analytical solution for bearing capacity factor using modified Hoek-Brown failure criterion", *Can. Geotech. J.*, https://doi.org /10.1139/cgj-2016-0694.

Yang, X.L. and Yao, C. (2018), "Stability of tunnel roof in nonhomogeneous soils", *Int. J. Geomech.*, https://doi.org /10.1061/(ASCE)GM.1943-5622.0001104.

Yang, X.L. and Zhang, R. (2017), "Collapse analysis of shallow tunnel subjected to seepage in layered soils considering joined effects of settlement and dilation", *Geomech. Eng.*, **13**(2), 217-235.

Yang, X.L., Li, Z.W., Liu, Z.A. and Xiao, H. B. (2017), "Collapse analysis of tunnel floor in karst area based on Hoek-Brown rock media", *J. Centr. South U.*, **24**(4), 957-966.

Zhang, Y. (2015), "Effect of hydraulic distribution form on the stability of a plane slide rock slope under the nonlinear Barton-Bandis failure criterion", *Geomech. Eng.*, **8**(3), 391-414.

Zheng, D.F., Nian, T.K., Liu, B., Yin, P. and Song, L. (2015), "Coefficient charts for active earth pressures under combined loadings", *Geomech. Eng.*, **8**(3), 461-476.

JS

Appendix

$$f_1=\frac{1}{2}[e^{(\theta-\theta_0)\tan\varphi}+\frac{r_0^{'}}{r_0}e^{-(\theta-\theta_0)\tan\varphi}]$$

$$f_2=\frac{1}{2}[e^{(\theta-\theta_0)\tan\varphi}-\frac{r_0^{'}}{r_0}e^{-(\theta-\theta_0)\tan\varphi}]$$

$$f_3=\frac{\sin\theta_0}{\sin\theta}-\frac{1}{2}\left[e^{(\theta-\theta_0)\tan\varphi}+\frac{r_0^{'}}{r_0}e^{-(\theta-\theta_0)\tan\varphi}\right]=\frac{\sin\theta_0}{\sin\theta}-f_1$$

$$f_4=\frac{\sin\theta_0\sin(\theta_B+\beta_1)}{\sin\theta_B\sin(\theta+\beta_1)}-\frac{1}{2}\left[e^{(\theta-\theta_0)\tan\varphi}+\frac{r_0^{'}}{r_0}e^{-(\theta-\theta_0)\tan\varphi}\right]=\frac{\sin\theta_0\sin(\theta_B+\beta)}{\sin\theta_B\sin(\theta+\beta)}-f_1$$

$$f_5=\frac{1}{3(1+9\tan^2\varphi_t)}[(3\tan\varphi\cos\theta_h+\sin\theta_h)e^{3(\theta_h-\theta_0)\tan\varphi}-(3\tan\varphi\cos\theta_0+\sin\theta_0)]$$

$$f_6=\frac{1}{6}\frac{L}{r_0}(2\cos\theta_0-\frac{L}{r_0})\sin\theta_0$$

$$f_7=\frac{1}{6}e^{(\theta_h-\theta_0)\tan\varphi}[\sin(\theta_h-\theta_0)-\frac{L}{r_0}\sin\theta_h][\cos\theta_0-\frac{L}{r_0}+\cos\theta_h e^{(\theta_h-\theta_0)\tan\varphi}]$$

$$\begin{aligned}g_1&=2\int_{\theta_0}^{\theta_B}\int_0^{\alpha_1^*}f_2(f_1+f_2\cos\alpha)^2d\alpha d\theta\\&=\int_{\theta_0}^{\theta_B}f_2(2f_1^2+f_2^2)arccos(f_3/f_2)d\theta+\int_{\theta_0}^{\theta_B}f_2(4f_1+f_3)\sqrt{f_2^2-f_3^2}d\theta\end{aligned}$$

$$\begin{aligned}g_2&=2\int_{\theta_0}^{\theta_h}\int_0^{\alpha_1^*}f_2^2(\cos\alpha-\cos\alpha_1^*)(f_1+f_2\cos\alpha)^2\sin\theta d\alpha d\theta\\&=\int_{\theta_0}^{\theta_h}\left[arccos(f_3/f_2)(2f_1f_2^3-2f_1^2f_2f_3-f_2^3f_3)+\sqrt{f_2^2-f_3^2}\left(2f_1^2f_2-2f_1f_2f_3+\frac{4}{3}f_2^3-\frac{1}{3}f_2f_3^2\right)\right]\sin\theta d\theta\end{aligned}$$

$$\begin{aligned}g_3&=2\int_{\theta_B}^{\theta_h}\int_0^{\alpha_2^*}f_2(f_1+f_2\cos\alpha)^2d\alpha d\theta\\&=\int_{\theta_B}^{\theta_h}f_2(2f_1^2+f_2^2)arccos(f_4/f_2)d\theta+\int_{\theta_B}^{\theta_h}f_2(4f_1+f_4)\sqrt{f_2^2-f_4^2}d\theta\end{aligned}$$

$$\begin{aligned}g_4&=2\int_{\theta_B}^{\theta_h}\int_0^{\alpha_2^*}f_2(f_1+f_2\cos\alpha)^2f_6d\alpha d\theta\\&=\int_{\theta_B}^{\theta_h}f_2f_6(2f_1^2+f_2^2)arccos(f_4/f_2)d\theta+\int_{\theta_B}^{\theta_h}f_2f_6(4f_1+f_4)\sqrt{f_2^2-f_4^2}d\theta\end{aligned}$$

$$\begin{aligned}g_5&=2\int_{\theta_B}^{\theta_h}\int_0^{\alpha_2^*}f_2^2(\cos\alpha-\cos\alpha_2^*)(f_1+f_2\cos\alpha)^2\sin\theta d\alpha d\theta\\&=\int_{\theta_B}^{\theta_h}\left[arccos(f_4/f_2)(2f_1f_2^3-2f_1^2f_2f_4-f_2^3f_4)+\sqrt{f_2^2-f_4^2}\left(2f_1^2f_2-2f_1f_2f_4+\frac{4}{3}f_2^3-\frac{1}{3}f_2f_4^2\right)\right]\sin\theta d\theta\end{aligned}$$

$$g_6=\frac{b}{H}\frac{1}{2\tan\varphi}\left[e^{(\theta_h-\theta_0)\tan\varphi}\sin\theta_h-\sin\theta_0\right]\left\{\exp\left[2(\theta_h-\theta_0)\tan\varphi\right]-1\right\}$$

$$\begin{aligned}g_7=&-\frac{b}{H}\frac{\lambda}{2\tan\varphi}\left[e^{(\theta_h-\theta_0)\tan\varphi}\sin\theta_h-\sin\theta_0\right]\sin\theta_0\left\{\exp\left[2(\theta_h-\theta_0)\tan\varphi\right]-1\right\}\\&+\frac{b}{H}\lambda\left[e^{(\theta_h-\theta_0)\tan\varphi}\sin\theta_h-\sin\theta_0\right]\cdot\\&\frac{3\tan\varphi\left\{\sin\theta_h\exp\left[3(\theta_h-\theta_0)\tan\varphi\right]-\sin\theta_0\right\}+\cos\theta_0-\cos\theta_h\exp\left[3(\theta_h-\theta_0)\tan\varphi\right]}{9\tan^2\varphi}\end{aligned}$$

$$\begin{aligned}g_8=&2\int_{\theta_0}^{\theta_B}[(f_2^2f_3/8-f_3^3/4-2f_1f_3^2/3-f_3f_1^2/2+2f_1f_2^2/3)\sqrt{f_2^2-f_3^2}\\&+(f_2^4/8+f_2^2f_1^2/2)\arcsin(\sqrt{f_2^2-f_3^2}/f_2)]\cos\theta d\theta\\&+2\int_{\theta_B}^{\theta_h}[(f_2^2f_4/8-f_4^3/4-2f_1f_4^2/3-f_4f_1^2/2+2f_1f_2^2/3)\sqrt{f_2^2-f_4^2}\\&+(f_2^4/8+f_2^2f_1^2/2)\arcsin(\sqrt{f_2^2-f_4^2}/f_2)]\cos\theta d\theta\end{aligned}$$

$$g_9=\frac{b}{H}(f_5-f_6-f_7)[\sin\theta_h e^{(\theta_h-\theta_0)\tan\varphi}-\sin\theta_0]$$

where in the Appendix:

Equations from f_1 to f_3 and equations from g_1 to g_2 for the calculation of internal energy dissipation $D_{AB\text{-}3D}$;

Equation f_4 and equations from g_3 to g_5 for the calculation of internal energy dissipation $D_{BC\text{-}3D}$;

Equations g_6 and g_7 for the calculation of internal energy dissipation $D_{\text{insert-}3D}$;

Equation g_8 for the calculation of external work rate $W_{\gamma\text{-}3D}$;

Equations from f_5 to f_7 and equation g_9 for the calculation of external work rate $W_{\gamma\text{-insert}}$.